Sharp bursts of high-flux reactive species in submicrosecond atmospheric pressure glow discharges

Sharp bursts of high-flux reactive species in submicrosecond atmospheric pressure glow discharges

J. L. Walsh and M. G. Kong[a)]
*Department of Electronic and Electrical Engineering, Loughborough University, Loughborough,
Leicestershire LE11 3TU, United Kingdom*

In this letter, the authors present an experimental study of the temporal characteristics of submicrosecond pulsed atmospheric glow discharges. Using electrical measurements and nanosecond-resolved optical emission spectroscopy, they show that a long initial period of each voltage pulse is spent building up space charges and is then followed by a large current pulse in the voltage-falling phase. Reactive plasma species such as oxygen atoms and OH radicals are produced in a train of sharp and independent pulses of 50–100 ns wide. Finally, their production is shown to increase significantly as the voltage pulse width reduces or the repetition frequency increases. © 2006 American Institute of Physics. [DOI: 10.1063/1.2397570]

With an immense application potential, atmospheric pressure glow discharges (APGDs) have recently commanded much attention.[1] A vast majority of APGD are generated with sinusoidal excitation at frequencies of typically 1–100 kHz (Refs. 2–5) and 1–60 MHz.[6–10] Much less studied are APGD generated by high-voltage pulses with pulse width of 0.5–100 μs and at a repetition frequency of a few kilohertz.[11–14] Compared to sinusoidal APGD, pulsed APGD tend to have low gas temperature,[11,14] high discharge current,[12–14] and high electrical efficiency.[11,14] They are particularly desirable for applications where wall-plug efficiency or/and room-temperature processing are critical, for example industrial-scale surface treatment[15] and food decontamination.[16] In a recent study, we reported a 1 kHz APGD generated with 360 ns high-voltage pulses between two naked electrodes.[17] With a large current density of 0.8 A/cm^2, the pulsed APGD was shown to produce far more intense atomic oxygen emission line at 777 nm than a comparable atmospheric dielectric-barrier discharge (DBD).[17] This is significant, given that reactive species such as atomic oxygen and OH radicals are key application enablers.[14–16,18] Therefore, it is of considerable interest to better understand and further develop pulsed APGD. In this letter, we present an experimental study of temporal characteristics of submicrosecond pulsed APGD and their generation of reactive plasma species under different pulsing conditions.

The submicrosecond pulsed APGD used for this investigation employed two parallel stainless-steel electrodes with a surface area of 6 cm^2 and a separation distance of 0.5 cm nominal. The two electrodes were naked without any dielectric barriers, and the electrode unit was housed within a Perspex box fed with a through flow of helium-oxygen mixture. Helium flow rate was fixed at 7 SLM (standard liters per minute) and oxygen flow rate at 10 SCCM (SCCM denotes cubic centimeter per minute at STP). The Perspex box was not air tight, and so ambient oxygen and nitrogen were present. A homemade power source provided a train of unipolar voltage pulses of up to 15 kV at 0.01–20 kHz. The

peak value of the voltage pulses was an adjustable input parameter, and the pulse duration was determined largely by the interaction of the power supply with the plasma. When the plasma current became sufficiently large, it increased the electrical conductivity of the gas gap critically to cause a sharp fall of the output voltage. Current and voltage were measured with a wideband current probe (Tektronix P6021), a wideband voltage probe (Tektronix P6015A), and a high-speed oscilloscope (Tektronix TDS 3000B). To allow for nanosecond-resolved spectral measurement, a pulse generator was used for triggering. Optical emission spectra were measured by an Andor Shamrock spectrometer with a focal length of 0.3 m and a grating of 600 grooves/mm.

Figure 1(a) shows electrical measurements of a 4 kHz submicrosecond pulsed APGD. The mean peak voltage is $V_p = 2.4$ kV, the peak discharge current is $I_p = 8.4$ A, and the peak dissipated power is 13.7 kW. Similar to those reported previously,[17] nanosecond plasma images suggest that the pulsed atmospheric plasma was spatially uniform without unstable streamers and its spatial structure had a clear sheath region (image not shown). Electrode temperature measured with a thermocouple was found to increase about 2 °C above room temperature. These observations confirm that it was an atmospheric pressure glow discharge. Compared to sinusoidal atmospheric DBD and indeed radio-frequency APGD, the pulsed APGD can be operated at very high peak power
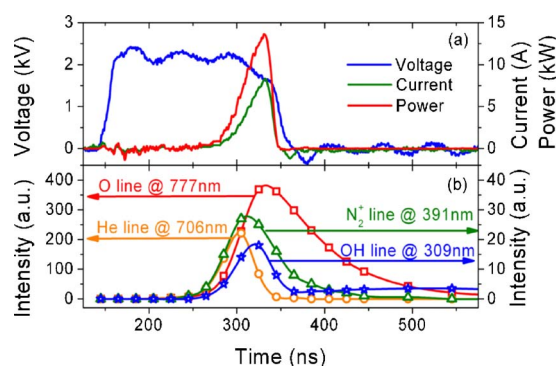

FIG. 1. (Color online) Characteristics of a submicrosecond APGD with (a) electrical measurement and (b) nanosecond-resolved optical emission of key plasma species.

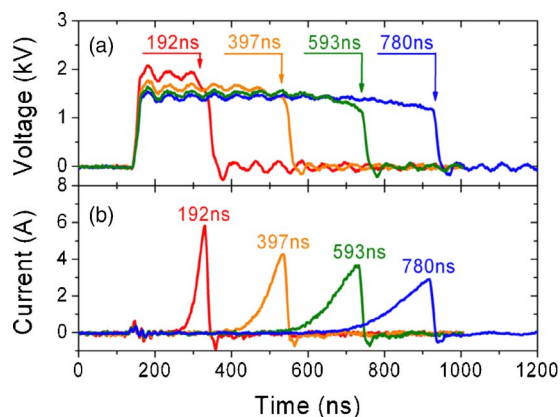a)Author to whom correspondence should be addressed; electronic mail:
m.g.kong@lboro.ac.uk

FIG. 2. (Color online) (a) Applied voltage and (b) discharge current of a submicrosecond APGD with four different voltage pulse widths.
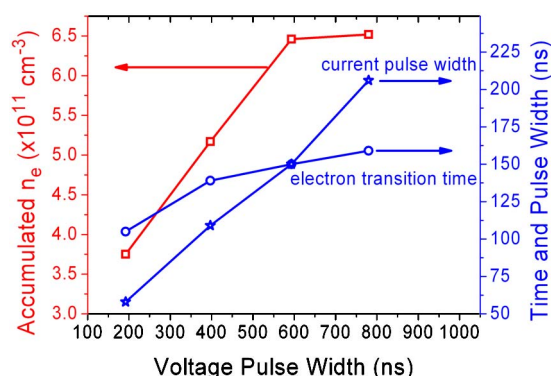

FIG. 3. (Color online) Pulse width dependence of the time-accumulated electron density over 1 V pulse, the electron transition time across the electrode gap, and the current pulse width measured between two $0.1I_p$ points.

density of $1-5$ kW/cm^3 without inducing any significant temperature rise. Figure 1(a) shows that its voltage pulse has a rise time of 18 ns and a fall time of 55 ns, both measured between 10% and 90% of the peak voltage, and a pulse width of $\Delta_v=190$ ns measured as the full width at half maximum. The current pulse has a rise time of 43 ns, a fall time of 10 ns, and a pulse width of $\Delta_c=30$ ns. With a voltage risetime of 18 ns and a rig capacitance of 1.1 pF, the peak displacement current is 0.15 A and much less than the peak current of 8.4 A. Therefore, the discharge current shown in Fig. 1(a) is likely to be the conduction current.

The discharge current pulse occurs in the voltage-falling phase, most probably because the electric field setup during the voltage-rising phase is insufficient to trigger gas ionization.[17] For helium APGD, it has been reported that the electric field must exceed a threshold of about 5.9 kV/cm in order to compensate electrons lost with electrons created.[19] During the voltage-rising phase, the peak electric field is unlikely to be much above 2.4 kV/0.5 cm=4.8 kV/cm. Markedly below the 5.9 kV/cm threshold, this is insufficient to trigger electron avalanche and so explains why no current peak is observed in the voltage-rising phase. It is worth mentioning that the short voltage pulse width prevents the generated electrons from reaching the anode. Assuming a peak electric field of 4.4 kV/cm and an electron mobility of 1132 cm^2 V^{-1} s^{-1} for the helium-oxygen mixture,[17] the time for an electron to cross the 0.5 cm electrode gap is found to be 100 ns—about 53% of the voltage pulse width. During the initial period of 100 ns, the generated electrons are trapped in the electrode gap and contribute to the buildup of space charges. This charge-accumulating period of 100 ns is similar to the time difference of $\Delta t_{onset}=127$ ns in the onset instant between the voltage and current pulses. In other words, a large portion of the voltage pulse is spent building up space charges so that the maximum electric field is raised above the breakdown electric field and triggers an electron avalanche.

The above discussion is supported by results of optical emission spectroscopy. It is known that the 391 nm line contains the optical signature of helium metastables and molecular helium ions.[20] It is also known that the 706 nm line is linked to either energetic electrons or He$_2^+$ and low energy electrons.[20] As the most numerous ions in helium APGD are molecular helium ions,[21] the temporal profiles of the 391 and 706 nm lines follow the profile of space charges. As shown in Fig. 1(b), emission line intensities at 391 and 706 nm are

negligible in the first 122 ns of the voltage pulse and so initially there are very few space charges in the gas gap to sustain a large current. The negligible emission period of 122 ns agrees very well with $\Delta t_{onset}=127$ ns.

Figure 1(b) also shows a pulse of the OH line at 309 nm and a pulse of the oxygen atom line at 777 nm, with their pulse widths being 60.0 and 106.3 ns, respectively. When compared to an atmospheric DBD using the same electrode unit, the same background gas and a very similar peak voltage, the intensities of the 307 and 777 nm emission lines in the pulsed APGD are up to ten times greater (data not shown). Therefore, a distinct character of submicrosecond pulsed APGD is their ability to produce high fluxes of reactive plasma species such as oxygen atoms and OH radicals. At a repetition frequency of 4 kHz, the half period is 125 μs and much longer than the electron transition time of $\tau_e=100$ ns across the electrode gap. Therefore, electrons generated in one voltage pulse are most certainly lost to the electrodes and through ionic recombination well before the next voltage pulse. This suggests that reactive plasma species such as oxygen atoms and OH radicals are generated as a train of sharp and independent bursts. It is conceivable that such submicrosecond windows of high-flux reactive species could facilitate surface modification with spatial or/and temporal selectivity. For example, a surface pattern with sharp boundaries could be realized by moving a pulsed APGD jet over a surface at a speed that translates the time scale of the windows to spatial dimensions of the surface pattern.

To enhance the production of reactive plasma species, we altered the peak applied voltage so as to alter the discharge current. As the peak applied voltage increases, Fig. 2 shows that the peak discharge current increases but the voltage pulse width decreases. The peak current I_p is very high, ranging from 3 to 6 A, and corresponds to a current density of $0.5-1.0$ A/cm^2. It is probable that such a high discharge current could substantially increase electrical conductivity of the gas to short-circuit the gas gap, leading to a premature shortening of the voltage pulse. To study this further, we integrated the current pulses in Fig. 2(b) to obtain the total accumulated electron density generated during each voltage pulse. This is shown in Fig. 3 together with the electron transition time across the electrode gap τ_e and the current pulse width Δ_c, the latter now being measured between the two $0.1I_p$ points to be comparable to the accumulated electron density that is obtained by integrating over the entire current pulse. While the voltage pulse width varies by a fac-
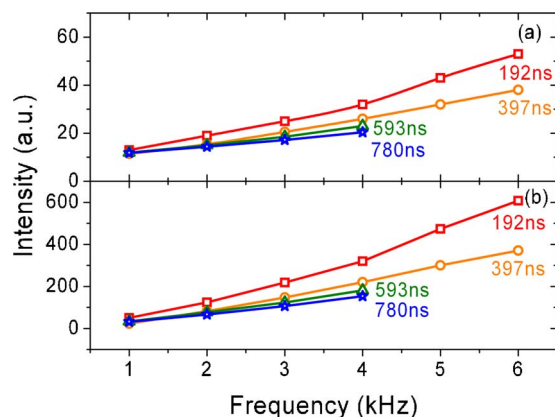
FIG. 4. (Color online) Frequency dependence of emission intensity of (a) the OH line at 309 nm and (b) the atomic oxygen line at 777 nm.

FIG. 5. (Color online) Frequency dependence of (a) the average dissipated power and (b) the peak electrical power.

tor of more than 4, the total accumulated electron density varies only by a factor of 1.7 suggesting similar gas conductivity among all four cases. At $\Delta_v = 192$ ns, τ_e is 106 ns and Δ_c is 58 ns. Therefore during the current pulse, most generated electrons are unable to reach the anode and so are trapped in the gas gap. In this case, the accumulated electron density is likely to be close to the peak electron density of 3.6×10^{11} cm^{-3} in the gas gap. At $\Delta_v = 397$ ns, $\tau_e = 139$ ns and $\Delta_c = 109$ ns. As $\tau_e < \Delta_c$ and they are now comparable, many generated electrons are trapped in the gas gap but the trapped electrons are proportionally fewer than those in the $\Delta_v = 192$ ns case. As a result, the peak electron density achieved during the current pulse is smaller than the accumulated electron density of 5.1×10^{11} cm^{-3} in Fig. 3. As Δ_v increases to 593 ns, both τ_e and Δ_c become 150 ns. This suggests that a significant proportion of generated electrons are now lost to the electrodes and the peak electron density reached during the current pulse is likely to be markedly smaller than the accumulated electron density of 6.5×10^{11} cm^{-3}. This difference is greater in the case of $\Delta_v = 780$ ns, for which $\tau_e = 159$ ns is now less than $\Delta_c = 206$ ns. Therefore as Δ_v increases, the peak electron density achieved during a current pulse becomes progressively less than its corresponding accumulated electron density in Fig. 3. This suggests that the peak electron density and hence the maximum electrical conductivity of the gas gap change little during the current pulse for all four cases of Fig. 3. It is therefore highly likely that narrow voltage pulse width at large voltage is caused by plasma-induced short circuiting of the gas gap.

Figure 4 shows that the optical emission intensity of OH line at 309 nm and atomic oxygen line at 777 nm for the four different voltage pulse widths. At a fixed frequency, stronger emission intensity is achieved with shorter pulse width that is linked to a large peak current (see Fig. 2). At a given Δ_v, the emission intensity increases with increasing frequency. At $\Delta_v = 192$ ns, the 777 nm line intensity increases by a factor of 12 as the frequency increases from 1 to 6 kHz. A high frequency leads to more frequent production of sharp bursts of reactive plasma species and so to their greater accumulation over a given time period. Also at long voltage pulsewidth of $\Delta_v = 593$ and 780 ns, stable APGDs are achieved only at frequencies up to 4 kHz. If Δ_v is reduced to below 400 ns,
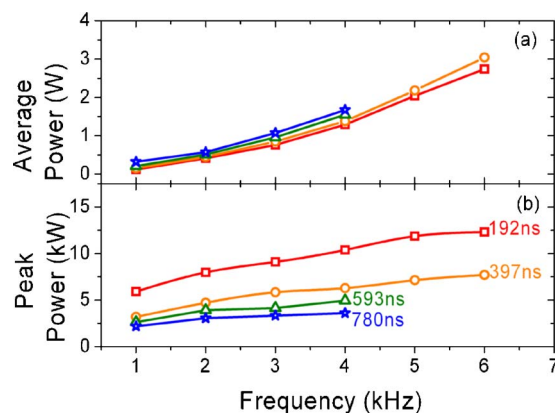
stable APGD can be extended to above 6 kHz.

To place the above comparison in the context of energy budget, the average dissipated power is shown in Fig. 5 to increase with the frequency but change little with voltage pulse width. Combining this result with those in Fig. 4, it is clear that production of oxygen atoms and OH radicals can be increased substantially without consuming more electrical power. The peak power is very large, particularly with short voltage pulse width. This is useful to sustain a large current and a large flux of reactive plasma species.

[1] J. R. Roth, *Industrial Plasma Engineering* (Institute of Physics, Philadelphia, 1995), Vol. 1, pp. 453–460.
[2] S. Kanazawa, M. Kogoma, T. Moriwaki, and S. Okazaki, J. Phys. D **21**, 838 (1988).
[3] F. Massines and G. Gouda, J. Phys. D **31**, 3411 (1998).
[4] I. Radu, R. Bartnikas, and M. R. Wertheimer, IEEE Trans. Plasma Sci. **31**, 411 (2003).
[5] X. T. Deng and M. G. Kong, IEEE Trans. Plasma Sci. **32**, 1709 (2004).
[6] S. E. Babayan, J. Y. Jeong, V. J. Tu, J. Park, G. S. Selwyn, and R. F. Hicks, Plasma Sources Sci. Technol. **7**, 286 (1998).
[7] J. J. Shi, X. T. Deng, R. Hall, J. D. Punnet, and M. G. Kong, J. Appl. Phys. **94**, 6303 (2003).
[8] L. Baars-Hibbe, C. Schrader, P. Sichler, T. Cordes, K. H. Gericke, S. Buttgenbach, and S. Draeger, Vacuum **73**, 327 (2004).
[9] Z. Yu, K. Hoshimiya, J. D. Williams, S. F. Polvinen, and G. J. Collins, Appl. Phys. Lett. **83**, 854 (2003).
[10] J. J. Shi and M. G. Kong, Phys. Rev. Lett. **96**, 105009 (2006).
[11] M. G. Kong and X. T. Deng, IEEE Trans. Plasma Sci. **31**, 7 (2003).
[12] M. Laroussi, X. Liu, V. Kolobov, and R. Arslanbekov, J. Appl. Phys. **96**, 3028 (2004).
[13] M. Laroussi, X. Liu, V. Kolobov, and R. Arslanbekov, J. Appl. Phys. **96**, 3028 (2004).
[14] J. L. Walsh, J. J. Shi, and M. G. Kong, Appl. Phys. Lett. **88**, 171501 (2006).
[15] J. R. Roth, Phys. Plasmas **12**, 057103 (2005).
[16] M. Vleugels, G. Shama, X. Deng, E. Greenacre, T. Brocklehurst, and M. G. Kong, IEEE Trans. Plasma Sci. **33**, 824 (2005).
[17] J. L. Walsh, J. J. Shi, and M. G. Kong, Appl. Phys. Lett. **89**, 161505 (2006).
[18] M. Moravej, X. Yang, R. F. Hicks, J. Penelon, and S. E. Babayan, J. Appl. Phys. **99**, 093395 (2006).
[19] J. Shi and M. G. Kong, Appl. Phys. Lett. **86**, 091502 (2005).
[20] G. Nersisyan and W. G. Graham, Plasma Sources Sci. Technol. **13**, 582 (2004).
[21] J. J. Shi and M. G. Kong, J. Appl. Phys. **97**, 023306 (2005).